The influence of the void environment on the ratio of dark matter halo mass to stellar mass in SDSS MaNGA galaxies

KELLY A. DOUGLASS, 1 JACOB A. SMITH, 1 AND REGINA DEMINA 1

<sup>1</sup> Department of Physics & Astronomy, University of Rochester, 500 Wilson Blvd., Rochester, NY 14611

#### ABSTRACT

We study how the void environment affects the formation and evolution of galaxies in the universe by comparing the ratio of dark matter halo mass to stellar mass of galaxies in voids with galaxies in denser regions. Using spectroscopic observations from the SDSS MaNGA DR15, we estimate the dark matter halo mass of 641 void galaxies and 937 galaxies in denser regions. We use the velocity from the H $\alpha$  emission line to measure the rotation curve of the galaxies since the kinematics of the interstellar medium is smoother than the stellar kinematics. We find that neither the stellar-to-halo-mass relation nor the relationship between the gas-phase metallicity and the ratio of dark matter halo mass to stellar mass is affected by the void environment. We also observe no difference in the distribution of the ratio of dark matter halo mass to stellar mass between void galaxies and galaxies in denser regions, implying that the shape of the dark matter halo profile is independent of a galaxy's environment.

Keywords: cosmology: dark matter — galaxies: spiral — galaxies: structure

### 1. INTRODUCTION

As shown by large galaxy redshift surveys, the large-scale structure of the universe is well described as a three-dimensional cosmic web (Bond et al. 1996): thin filaments of galaxies connect galaxy clusters and surround voids. These voids are large, under dense regions of space that occupy close to 60% of the volume of the universe (da Costa et al. 1988; Geller & Huchra 1989; Pan et al. 2012). Over the last couple of decades, the Sloan Digital Sky Survey (SDSS; York et al. 2000) has provided an unprecedented data set which has made possible the study of the influence of the large-scale environment on the formation and evolution of galaxies.

Cosmic voids are an important environment for studying galaxy formation (see van de Weygaert & Platen 2011, for a review) because the gravitational clustering within them proceeds as if in a very low-density universe. According to the  $\Lambda$ CDM cosmology, galaxies formed in voids should have lower masses and be retarded in their star formation when compared to those in more dense environments (Gottlöber et al. 2003; Goldberg et al. 2005; Cen 2011).

Previous studies of the properties of void galaxies have found that their characteristics differ from

Corresponding author: Kelly A. Douglass kellyadouglass@rochester.edu

galaxies which reside in denser environments. In general, void galaxies have lower stellar mass (Hoyle et al. 2005; Croton et al. 2005; Moorman et al. 2015), are bluer and of a later type (Grogin & Geller 2000; Rojas et al. 2004; Patiri et al. 2006; Park et al. 2007; von Benda-Beckmann & Müller 2008; Hoyle et al. 2012), have higher specific star formation rates (Rojas et al. 2005; von Benda-Beckmann & Müller 2008; Moorman et al. 2015; Beygu et al. 2016), and are more gas rich (Kreckel et al. 2012) than galaxies in denser regions.

The ratio of dark matter halo mass to stellar mass in a galaxy should affect the properties that depend on a galaxy's gravitational potential well. Deeper potential wells prevent a higher fraction of gas from escaping the galaxy due to supernova-driven winds, tidal stripping, etc. The gas-phase metallicity of a galaxy (defined as the relative abundance of oxygen relative to hydrogen,  $12 + \log(O/H)$ ) is a measure of the integrated star formation history of a galaxy. Galaxies typically follow the mass-metallicity relation (Tremonti et al. 2004), where more massive galaxies have higher metallicities. While a galaxy's metallicity should depend on its stellar mass, it should also increase with its total mass due to the corresponding deeper potential well.

Void galaxies are expected to have lower gas-phase metallicities than those in denser regions if they only recently started forming stars or have recently accreted unprocessed gas. However, Mouhcine et al. (2007); Cooper et al. (2008); Nicholls et al. (2014);

Kreckel et al. (2015); Douglass & Vogeley (2017a,b) and Douglass et al. (2018) found that void dwarf galaxies do not have systematically lower gas-phase metallicities than dwarf galaxies in denser regions. Douglass & Vogeley (2017b) and Douglass et al. (2018) posit that this might be the result of larger ratios of dark matter halo mass to stellar mass in void galaxies. We aim to test this hypothesis by estimating the mass ratios for void galaxies and comparing them to the mass ratios of galaxies in denser regions.

The primary objective of this paper is to compare the ratios of dark matter halo mass to stellar mass in spiral galaxies to discern if the void environment has an influence on their mass composition. In this paper, we utilize the SDSS Data Release 15 (DR15; Aguado et al. 2019), which includes the most recent data from the SDSS MaNGA integral field spectroscopic survey (Bundy et al. 2015).

# 2. SDSS MANGA DATA AND GALAXY SELECTION

Unlike previous SDSS surveys, the SDSS MaNGA survey measures spectra across the face of each observed galaxy. Placing a bundle of spectroscopic fibers (an Integral Field Unit, IFU) that vary in size from 12" (19 fibers) to 32" (127 fibers) on each galaxy (Drory et al. 2015), MaNGA will collect spectra of 10,000 nearby galaxies in the northern sky by its conclusion. The IFUs are fed to two dual-channel spectrographs that simultaneously cover a wavelength range of 3600–10,300Å with a resolution of  $\lambda/\Delta\lambda \sim 2000$ . We use the H $\alpha$  velocity map, V-band image, and stellar mass density map as processed by Pipe3D (Sánchez et al. 2016, 2018), an analysis pipeline designed to investigate the properties of the stars and ionized gas in integral field spectroscopic data. Galactic inclination angles, axis ratios, and absolute magnitudes are taken from the NASA-Sloan Atlas (Blanton et al. 2011).

## 2.1. IFU spaxel mask

In order to filter out invalid spaxels, we apply a series of restrictions to the various data fields used. We mask those spaxels with an error in the  ${\rm H}\alpha$  velocity of either zero or not a number, a flux and/or error in the V-band of zero, and an estimate of zero for the stellar mass density. These requirements result in an average of 21% of spaxels masked in each galaxy. Of the 4815 galaxies processed by Pipe3D, 333 (6.9%) are completely masked.

We also remove those galaxies with noisy velocity maps by requiring galaxies to have a "smoothness" score less than 2.27. This score is determined by summing the cosine distance  $(1 - \cos \theta)$  across all unmasked spaxels and their four adjacent unmasked neighbors, where  $\theta$  is the angle between the spaxel's gradient and its neighbor's gradient. This sum is then normalized by the total number of unmasked spaxels in the velocity map. As described in Section 4.2, additional quality selection criteria are applied after fitting the rotation curves.

### 2.2. Environment classification

The large-scale environment for each galaxy is defined by the voids identified with VoidFinder (Hoyle & Vogeley 2002), an implementation of the void-finding algorithm described in El-Ad & Piran (1997), applied to a volume-limited sample of the SDSS DR7 galaxy catalog (Abazajian et al. 2009) with absolute magnitude  $M_r < -20$ . VoidFinder removes all isolated galaxies, defined as those separated from their third nearest neighbor by more than  $7h^{-1}$ Mpc. A grid is then applied to the remaining galaxies, and a sphere is grown from the center of each empty cell until it is bounded by four galaxies. Each sphere with a minimum radius of  $10h^{-1}$ Mpc can serve as a seed for a void. The sphere which seeds a void is referred to as that void's maximal sphere. To identify dynamically-distinct voids, maximal spheres are not permitted to overlap each other by more than 10% of their volume. If any of the remaining spheres overlap a maximal sphere by at least 50% of its volume, it adds to that maximal sphere's void; otherwise it is discarded. See Hoyle & Vogeley (2002) for a more detailed description of VoidFinder.

Galaxies that reside within a void are considered void galaxies; otherwise they are referred to as wall galaxies. Due to the finite survey footprint of SDSS DR7, we cannot locate voids within  $10h^{-1}{\rm Mpc}$  of the survey boundary. Any galaxy that falls within this border region or outside the survey footprint is classified as "Uncertain."

### 3. ESTIMATING THE MASS COMPONENTS

The rotation curve is a measure of the galaxy's spin rate as a function of distance from the galaxy's center. By measuring a galaxy's rotation curve, we can estimate the total mass of the galaxy. Assuming Newtonian mechanics, the rotation rate of the stars and gas a distance r from the center of the galaxy should only depend on the total enclosed mass within that distance, M(r). The following is an overview of the theory and method that we employ to estimate the galactic rotation curves in the MaNGA galaxies.

### 3.1. Newtonian mechanics

We assume that a galaxy's rotational motion is dominated by basic orbital mechanics: the orbital velocity of a particle some distance r from the center of the galaxy is a function of the total mass internal to that radius, M(r). For spiral galaxies, the orbital motion is assumed to be circular. The gravitational force is the source of the centripetal acceleration for a particle in orbit, so

$$M(r) = \frac{v(r)^2 r}{G} \tag{1}$$

Here, v(r) is the velocity a distance r from the center of the galaxy, and  $G = 6.67408 \times 10^{-11} \text{ m}^3 \text{ kg}^{-1} \text{ s}^{-2}$  is the Newtonian gravitational constant. Thus, by measuring v(r) and r, we can estimate M(r).

### 3.2. Separating the mass components

Observed galaxy rotation curves do not match what we would expect based on the visible matter distribution. If a galaxy's mass was composed entirely of baryonic matter, then its rotation curve would fall off as  $1/\sqrt{r}$  since photometric analysis indicates that the majority of a galaxy's baryonic mass is located within the central part of the galaxy. However, the observed galaxy rotation curves level out, indicating that there is an additional component of material that results in the mass distribution increasing with radius (Freeman 1970; Rubin & Ford 1970). This additional, unobserved material has been dubbed "dark matter," since it does not interact electromagnetically.

The rotation curve we measure from the data is a function of the total mass present within a given radius. We assume that the two main components of the mass composition are dark matter and stellar mass. Since the interstellar gas comprises only  $\sim 10\%$  of the disk's mass (Nakanishi & Sofue 2006), including its contribution to the rotation curve will decrease our calculated dark matter mass by a negligible amount. The difference between the total and stellar mass, evaluated using an independent estimate (see Section 4.3), is our estimate for the dark matter mass at a given radius.

## 4. ROTATION CURVE ANALYSIS AND RESULTS

### 4.1. Measuring galactic rotation curves

We use the velocity of the gas in the galaxy to determine its rotation curve, since gas kinematics are more continuous and less subject to random motions than the stellar population. An example of the  $H\alpha$  velocity map masked as described in Section 2.1 is shown in Figure 1. The velocities have been corrected to the internal motion of the galaxy by subtracting out the galaxy's center's velocity, and they have been deprojected by assuming that the photometric inclination is also the kinetic inclination across the entire galaxy. As done in

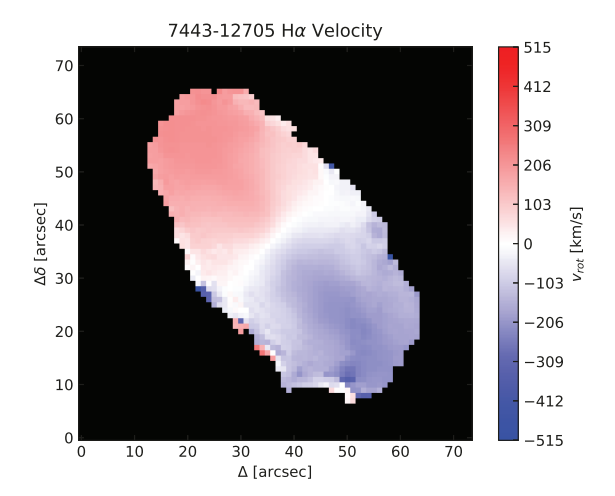


Figure 1. An example of the  $H\alpha$  velocity field corrected to the galaxy's rest frame. Blue spaxels represent a blue-shifted  $H\alpha$  velocity, while red spaxels represent a red-shifted  $H\alpha$  velocity. The mask described in Section 2.1 is applied.

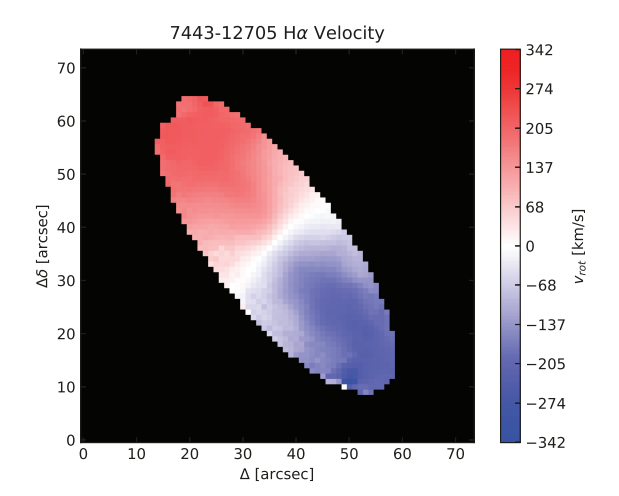


Figure 2. An example of the  $H\alpha$  velocity spaxels included in the analysis. Due to the galaxy's angle of inclination, the annuli are not necessarily circular from our perspective.

Barrera-Ballesteros et al. (2018), we assume that the kinetic and photometric centers of the galaxies are identical

By taking into account the galaxy's angle of inclination and axis ratio, we find the minimum and maximum velocities along a given annulus of the galaxy. This annulus corresponds to a circle centered on the galaxy's center when the galaxy is viewed face-on. An example of the final footprint of these annuli is shown in Figure 2.

From these velocities, we get a rotation curve for the side of the galaxy rotating towards us (the "negative"

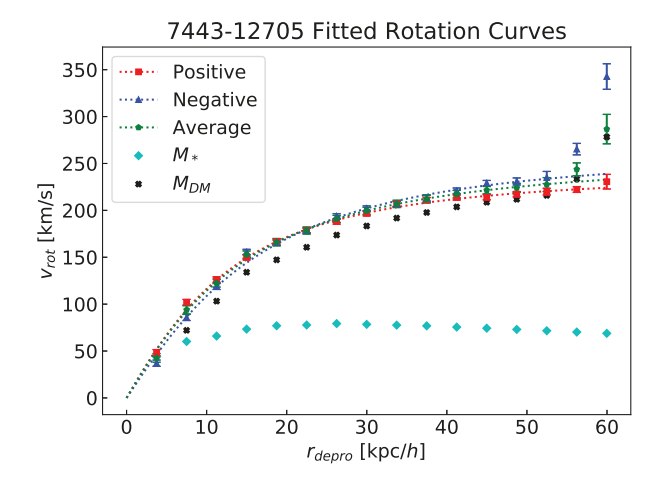


Figure 3. An example of the rotation curves for one galaxy. The rotation curve from the positive velocities is shown with red squares, the negative velocities with blue triangles, and the average velocity curve with green pentagons. Best fits for these three curves are shown in the corresponding colored dashed lines. The rotation curve due to the stellar mass component is shown in the teal diamonds. The rotation curve due to the estimated dark matter component is shown in the black  $\mathbf{x}$ 's.

curve), and a rotation curve for the side rotating away from us (the "positive" curve). We combine these two rotation curves by computing the average of the absolute value of the velocities at each deprojected radius to obtain a single rotation curve for the galaxy. An example of these curves for one galaxy are shown in Figure 3, with the rotation curve from the positive velocities drawn with red squares, the absolute value of the negative velocities with blue triangles, and the average velocity curve with green pentagons. We fit each of these rotation curves with the parameterization defined by Barrera-Ballesteros et al. (2018):

$$V_{\rm rot} = \frac{V_{\rm max} r_{\rm depro}}{(R_{\rm turn}^{\alpha} + r_{\rm depro}^{\alpha})^{1/\alpha}}$$
(2)

where  $V_{\rm rot}$  is the rotational velocity measured at a given deprojected radius  $r_{\rm depro}$ ,  $V_{\rm max}$  is the magnitude of the velocity on the plateau of the rotation curve, and  $R_{\rm turn}$  is the deprojected radius at which the curve plateaus. The free parameters in the fit are  $V_{\rm max}$ ,  $R_{\rm turn}$  and  $\alpha$ .

To confirm that Equation 2 successfully reproduces the form of the rotation curves for the galaxies in our sample, we plot the distribution of maximum velocities as a function of  $M_r$  (the Tully-Fisher relation; Tully & Fisher 1977). As seen in Figure 4, there is a strong positive correlation between the absolute magnitude and the maximum velocity, as expected.

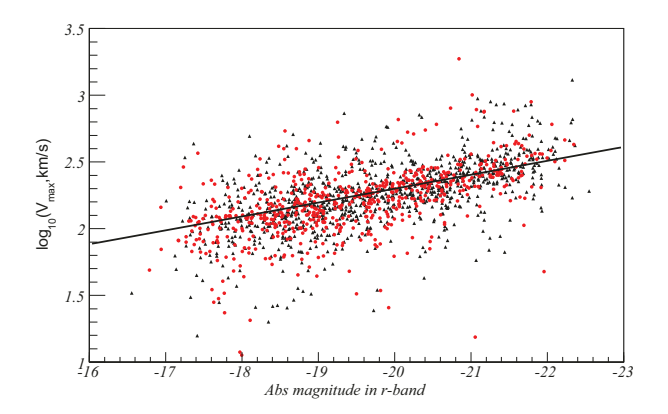


Figure 4. The logarithm of maximum velocity as a function of absolute magnitude in the r-band for void (red circles) and wall (black triangles) galaxies. The Tully-Fisher relation from Tully & Fisher (1977) is shown in the solid black line.

### 4.2. Best Fit Quality Cuts

We require that a galaxy's rotation curve contain at least four data points for the fitting procedure and analysis to proceed. In addition, we only include those galaxies with the goodness of fit of the rotation curve characterized by a reduced  $\chi^2$  ( $\chi^2_{\nu}$ ) < 10. Here,  $\chi^2_{\nu}$  is normalized by the difference of the number of data points in the fit and the number of degrees of freedom of the fit. If  $\chi^2_{\nu}$ is too large for the average rotation curve, the fit to the positive curve is checked. If it has a good fit  $(\chi^2_{\nu} < 10)$ , then the positive curve's fit is used for the analysis; if not, then the negative curve is checked. If none of these three fits has a  $\chi^2_{\nu}$  < 10, then the last data point in each of the rotation curve data are removed, and the fits are re-calculated. This procedure continues until either a good fit is found, or there are less than four data points remaining in the rotation curves, at which point the galaxy is removed from the sample.

Both this procedure and the removal of galaxies without smooth velocity maps (described in Section 2.1) preferentially eliminate galaxies with low dark matter content (for which a rotation curve is dominated by the bulge's mass) and elliptical galaxies (which lack organized rotational motion). Since most elliptical galaxies are extremely bright, this introduces a selection bias towards fainter magnitudes. Of the 4815 galaxies with IFU spectra available in the Pipe3D analysis of the SDSS DR15 MaNGA survey, we have rotation curves for 641 void galaxies and 937 wall galaxies. The number of galaxies with rotation curves classified as uncertain is 845.

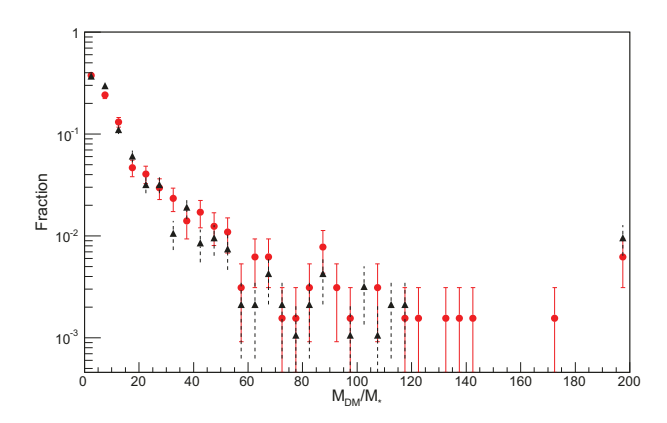


Figure 5. The distribution of the ratio of dark matter halo mass to stellar mass for void (red circles, solid line) and wall (black triangles, dotted line) galaxies. There is not a statistically significant difference in the distributions between the two environments.

## 4.3. Estimating the ratio of dark matter halo mass to stellar mass

The total mass internal to the galaxy is calculated using Equation 1, evaluated at the maximum deprojected radius measured in the rotation curves and using  $V_{\rm max}$  found from the best fit rotation curve of Equation 2.

In order to compute the total dark matter halo mass,  $M_{DM}$ , and total stellar mass,  $M_*$ , within a galaxy, we need to decompose the galaxy's rotation curve into its constituent parts. From the stellar mass densities, we can estimate the total stellar mass contained within a particular radius. From this mass distribution, we can calculate the expected rotation curve due to the stellar mass component of the galaxy. The rotation curve due to the stellar mass component is shown in the teal diamonds in Figure 3. By taking the stellar mass internal to the maximum deprojected radius, we can get an estimate of the discernible stellar mass in the galaxy.

Finally, the total dark matter halo mass for the galaxy is found by subtracting the total stellar mass estimated from the total mass calculated. The rotation curve due to the dark matter component of the sample galaxy can be found in Figure 3 as the black x's.

From this estimate of the total stellar mass and total dark matter halo mass observed for a given galaxy with this data set, we calculate the ratio of dark matter halo mass to stellar mass for each galaxy.

### 4.4. Distribution of $M_{DM}/M_*$

The distributions of the ratio of dark matter halo mass to stellar mass,  $M_{DM}/M_*$ , for void and wall galaxies used in this analysis are shown in Figure 5. There is no

Table 1. Sample sizes and the probability of  $\chi^2$  of the agreement between the distributions in the ratio of dark matter halo mass to stellar mass of the void and wall galaxies, binned by absolute magnitude as indicated on the left.

Range in $M_r$	Void	Wall	$P(\chi^2)$
All	641	937	0.78
Fainter than $-18$	81	79	0.99
Between $-18$ and $-19$	168	215	0.99
Between $-19$ and $-20$	166	244	0.99
Between $-20$ and $-21$	139	216	0.99
Brighter than $-21$	87	183	0.99

statistically significant difference in the distributions of  $M_{DM}/M_{\ast}$  between the two environments.

We acknowledge that  $M_{DM}/M_*$  has the potential to vary as a function of galaxy size, so we also look at the distributions when the galaxies are binned by absolute magnitude. Shown in Figure 6 and quantified in Table 1, the void environment does not affect the mass ratio distribution in any galaxy magnitude range. In Table 1, we present the sample size of the galaxies binned by their absolute magnitude and the probability of  $\chi^2$  of the difference in the distributions over  $M_{DM}/M_*$  between the void and wall galaxies. The lowest probability of  $\chi^2$ corresponds to the inclusive sample, where the median ratio of the dark matter halo mass to stellar mass is  $7.5\pm1.3$  in voids and  $7.1\pm1.2$  in walls. Once galaxies are binned by their absolute magnitude, their distributions in  $M_{DM}/M_*$  are even more consistent between the two environments.

### 4.5. Relationship between $M_{DM}/M_*$ and $M_r$

The relationship between  $M_{DM}/M_*$  and  $M_r$  (a form of the stellar-halo mass relation, SHMR) is shown in Figure 7. The distributions seen in Figure 6 show that fainter galaxies contain higher fractions of dark matter relative to their stellar mass content than brighter galaxies. This trend is shown more clearly in Figure 7, where we investigate the relationship between the median mass ratio in each magnitude bin. Fainter galaxies (those with  $M_r > -18$ ) have the highest  $M_{DM}/M_*$ , and the mass ratio decreases with the galaxies' magnitudes. These distributions show no statistically significant dependence on the environment.

In the brightest galaxies, we see that  $M_{DM}/M_*$  does not follow the trend present in the other magnitude bins. Instead, the mass ratio appears to either remain constant or increase slightly, indicating that the brightest

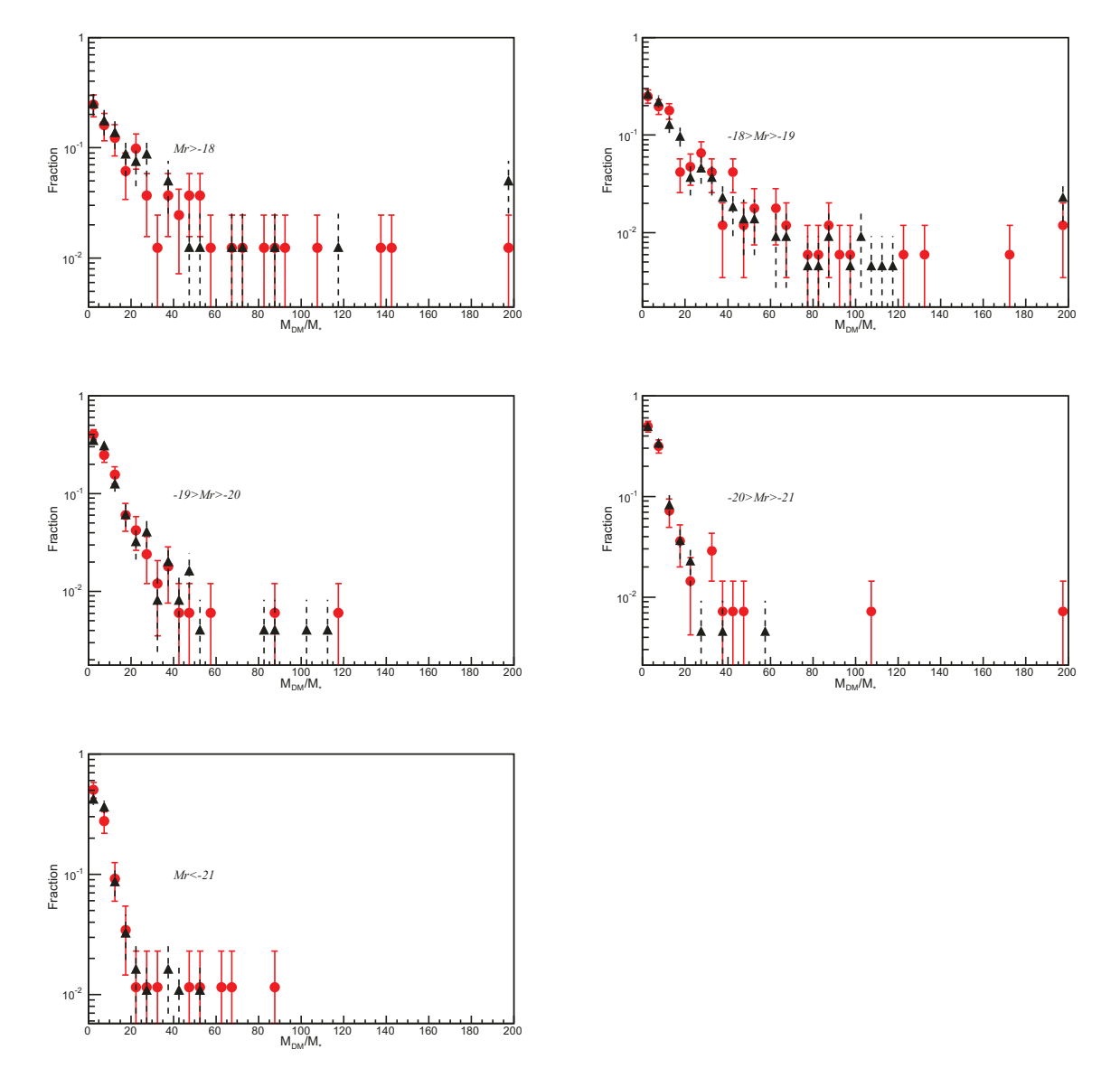


Figure 6. The distributions of  $M_{DM}/M_*$  for void (red circles, solid line) and wall (black triangles, dotted line) galaxies, binned by absolute magnitude. There is no statistically significant difference between the environments in any of the magnitude ranges.

galaxies  $(M_r < -21)$  have more dark matter halo mass relative to their stellar mass than slightly fainter galaxies. Similar trends are seen in Moster et al. (2010) and Di Paolo & Salucci (2018), where the SHMR is found to peak around  $\log(M_*/M_\odot) \sim 10.5$ .

The dependence of the median total mass and median stellar mass on the absolute magnitude are presented in Figure 8. As expected, both the total and stellar mass increase with galaxy brightness. The difference between the total mass and stellar mass in a magnitude bin corresponds to the dark matter halo mass. Figure 8 shows that this difference increases with decreasing brightness in all but the brightest galaxy bin, and the faintest galaxies have the largest difference between their

total mass and stellar mass. This matches the relationship we see in Figure 7, where the ratio of dark matter halo mass to stellar mass decreases with increasing brightness in all but the brightest magnitude bin.

It is well known (Hoyle et al. 2005) that void galaxies are characteristically fainter than wall galaxies. To confirm that our sample exhibits this characteristic, we show the normalized distributions in absolute magnitude in the two environments in Figure 9. Indeed, voids contain a higher fraction of faint galaxies than denser regions. Therefore, if  $M_{DM}/M_*$  depends on a galaxy's brightness, then the lower probability of  $\chi^2$  in the inclusive bin (Figure 5, first row of Table 1) is explained by the different distributions in the brightness of void and

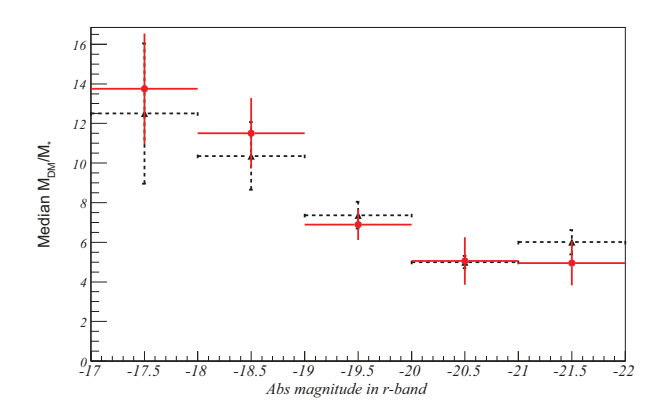


Figure 7. The median dark matter ratio as a function of absolute magnitude for void (red circles, solid line) and wall (black triangles, dotted line) galaxies. The fraction of dark matter decreases with increasing brightness in all but the brightest bins, independent of environment.

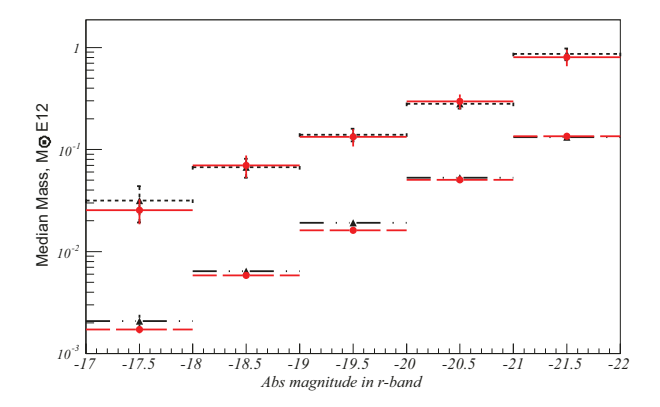


Figure 8. The median total mass (solid/dotted lines) and stellar mass (dashed/dot-dashed lines) as functions of absolute magnitude for void (red circles) and wall (black triangles) galaxies. Both the total mass and stellar mass increase with brightness, as expected.

wall galaxies. In general, there is a higher fraction of dwarf galaxies with higher dark matter content in the voids, while walls contain brighter galaxies with lower dark matter content.

# 5. THE INFLUENCE OF THE VOID ENVIRONMENT

### 5.1. Dark matter content of fainter galaxies

The well-known SHMR predicts and measures dwarf galaxies to have a higher fraction of dark matter than more massive galaxies (Wechsler & Tinker 2018, and references therein). Previous observations of the dwarf galaxies in the Local Group (Mateo 1998) indicate that there is an inverse correlation between the luminosity

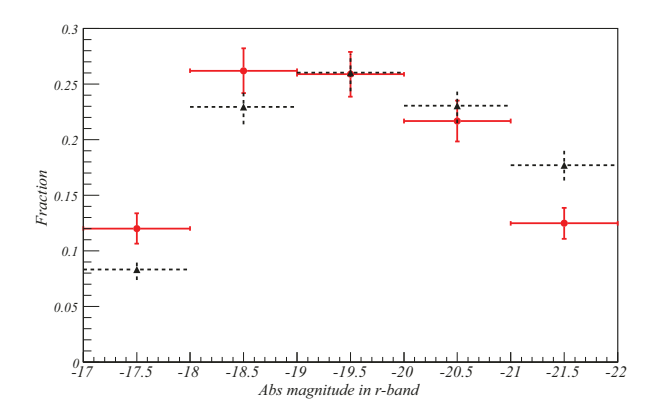


Figure 9. The distribution of void (red circles, solid line) and wall (black triangles, dotted line) galaxies in absolute magnitude. Void galaxies are characteristically fainter than galaxies found in denser regions.

and mass-to-light ratio in dwarf spheroidal galaxies. In addition, Torres-Flores et al. (2011) find that low-mass galaxies in the GHASP survey are dominated by dark matter, while those with higher masses are dominated by baryonic matter. Recent simulations by Martin et al. (2019) show that low surface brightness galaxies have a slightly higher fraction of dark matter compared to high surface brightness galaxies. Our results in Figure 7 align with the SHMR, where the relative fraction of dark matter increases with decreasing luminosity.

The deviation from a constant SHMR is suggested to be the result of various feedback processes which reduce the star formation efficiency: supernovae feedback in lower mass galaxies, and AGN feedback in the most massive galaxies (Di Paolo & Salucci 2018; Wechsler & Tinker 2018). We see no statistically significant effect from the void environment on the relationship between the median ratio of dark matter halo mass to stellar mass and the absolute magnitude, so the source of this relationship should not be influenced by the large-scale environment.

 $\Lambda {\rm CDM}$  cosmology predicts that star formation commenced at a later time in void galaxies than for galaxies in denser regions (Gottlöber et al. 2003; Goldberg et al. 2005; Cen 2011). If this is true, then the SHMR for void galaxies should be similar to that for galaxies in denser regions at an earlier redshift. The lack of a statistically significant difference in the relationships between the ratio of dark matter halo mass to stellar mass and the absolute magnitudes of galaxies in voids and in denser regions shown in Figure 7 aligns with the simulation results of Behroozi et al. (2019), who show that there is not much variance in the SHMR at redshifts  $z\lesssim 4$ .

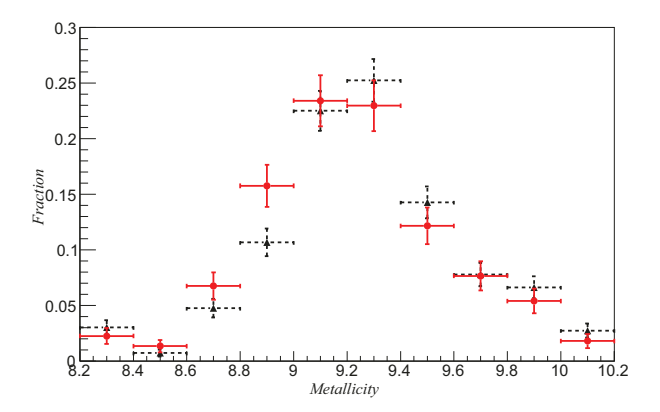


Figure 10. The gas-phase metallicity (12+log(O/H)) distribution for void (red circles, solid line) and wall (black triangles, dotted line) galaxies. The apparent shift toward lower metallicities in void galaxies is a result of the larger fraction of fainter galaxies in voids and the mass-metallicity relation.

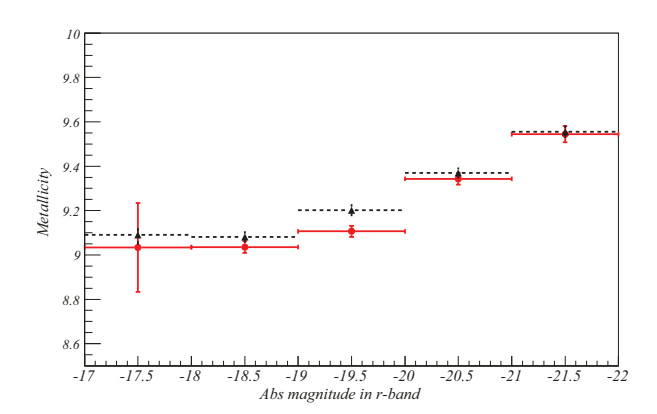


Figure 11. The average gas-phase metallicity (12 +  $\log(O/H)$ ) for galaxies binned by  $M_r$  for void (red circles, solid line) and wall (black triangles, dashed line) galaxies. The typical mass-metallicity relationship (increasing metallicity with absolute magnitude) is observed.

## 5.2. Implications for the gas-phase metallicity

The studies by Douglass & Vogeley (2017b) and Douglass et al. (2018) suggest that a shift towards higher  $M_{DM}/M_{\ast}$  in void galaxies could explain why void dwarf galaxies have gas-phase metallicities similar to dwarf galaxies in denser regions. However, as seen in Figures 5 and 6 and in Table 1, there is no statistically significant difference in the mass ratios for galaxies as a function of their large-scale environment.

Using the N2O2 diagnostic as calibrated by Brown et al. (2016), we calculate the gas-phase metallicities (12 +  $\log(O/H)$ ) of the galaxies in our sample using emission line flux values from the MPA-JHU value-added

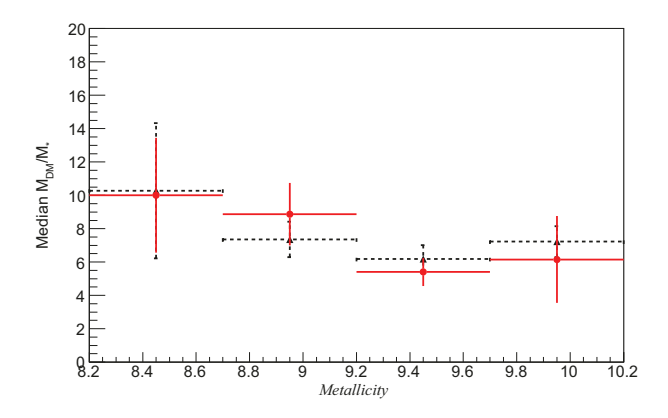


Figure 12. The ratio of dark matter halo mass to stellar mass as a function of gas-phase metallicity  $(12 + \log(O/H))$  for void (red circles, solid line) and wall (black triangles, dotted line) galaxies. As with the SHMR,  $M_{DM}/M_*$  decreases with increasing metallicity in all but the highest metallicity bin.

catalog<sup>1</sup>, which is based on the SDSS DR7 sample of galaxies. The distribution over metallicity is shown in Figure 10. The overall shift towards lower metallicities in the void galaxies is a result of the larger fraction of faint galaxies present in voids and the known mass-metallicity relation, shown in Figure 11.

We also study the dependence of  $M_{DM}/M_*$  on metallicity, shown in Figure 12. Due to the mass-metallicity relation (Figure 11) and the observed relationship between a galaxy's absolute magnitude and its dark matter fraction (Figure 7), we expect that galaxies with lower metallicities will have higher mass ratios. Indeed, this is what is shown in Figure 12, mimicking the relationship between  $M_r$  and  $M_{DM}/M_*$  seen in Figure 7. There is no statistically significant difference in the relationships between the gas-phase metallicity and  $M_{DM}/M_*$  of void galaxies and galaxies in denser regions. In general, galaxies with lower metallicities tend to have a higher fraction of dark matter.

### 5.3. Shape of the dark matter halo profile

If the dark matter halo profile is the same for void and wall galaxies, then any difference in the dark matter halo mass would be accounted for beyond the extent of the stellar disk. SDSS MaNGA only observes the visible baryonic matter in the galaxies, so we are not able to detect any differences beyond the extent of the stars. The dark matter halo mass estimates we calculate from these rotation curves provide a lower limit on the dark matter halo mass for these galaxies. As a result, we

<sup>&</sup>lt;sup>1</sup> Available at http://www.mpa-garching.mpg.de/SDSS/DR7/

would not see any difference in the ratio of dark matter halo mass to stellar mass in the MaNGA galaxies if the shape of the dark matter halo is the same.

If instead, the dark matter halo is more shallow in void galaxies (more pancake-shaped) than in wall galaxies, we would expect to see lower ratios of dark matter halo mass to stellar mass in the void dwarf galaxies with this data based on the conclusions of Douglass & Vogeley (2017b) and Douglass et al. (2018). Our results eliminate this potential geometry of the dark matter halo. If there is a difference in the halo profile of void galaxies, then it is in the extent of the halo beyond the luminous edge of the galaxy.

### 6. CONCLUSIONS

We investigate the influence of the void environment on the fraction of dark matter in galaxies by comparing the ratio of dark matter halo mass to stellar mass of galaxies in voids with galaxies in denser regions. Using the  ${\rm H}\alpha$  velocity maps from the SDSS MaNGA DR15, we are able to measure the rotation curves of 641 void galaxies and 937 galaxies in denser regions. From the rotation curves, we estimate the total mass of the galaxies; combined with the galaxies' stellar masses, we infer their dark matter halo masses.

We find that there is no difference in the ratio of dark matter halo mass to stellar mass in void galaxies and in galaxies in denser regions. We also do not find a statistically significant difference in either the relationship between the mass ratio and the absolute magnitude nor in the relationship between the gas-phase metallicity  $(12 + \log(O/H))$  and the mass ratio.

When separated by absolute magnitude, we find a general trend towards a decreasing ratio of dark matter halo mass to stellar mass with increasing absolute magnitude in all but the brightest galaxies. This relationship is independent of a galaxy's large-scale environment, so the SHMR does not appear to be affected by the void environment.

Because the MaNGA IFU only cover the extent of the luminous component of the galaxies, the dark matter halo masses that we estimate are lower limits on the total dark matter halo masses. Therefore, our results indicate that the dark matter halo profile is similar in void galaxies and in galaxies in denser regions. We cannot make any conclusions about the extent of the dark matter halo beyond the limit of the luminous matter. Further analysis with H I data, for example, would help

to discern any environmental affect on the extent of the dark matter halo.

#### 7. ACKNOWLEDGEMENTS

The authors would like to thank both Michael Vogeley for his insightful comments and Stephen W. O'Neill, Jr. for his help in determining the smoothness of the velocity maps. J.A.S. and R.D. acknowledge support from the Department of Energy under the grant DE-SC0008475.0.

This project makes use of the MaNGA-Pipe3D dataproducts. We thank the IA-UNAM MaNGA team for creating this catalogue, and the Conacyt Project CB-285080 for supporting them.

Funding for the Sloan Digital Sky Survey IV has been provided by the Alfred P. Sloan Foundation, the U.S. Department of Energy Office of Science, and the Participating Institutions. SDSS-IV acknowledges support and resources from the Center for High-Performance Computing at the University of Utah. The SDSS web site is www.sdss.org.

SDSS-IV is managed by the Astrophysical Research Consortium for the Participating Institutions of the SDSS Collaboration including the Brazilian Participation Group, the Carnegie Institution for Science, Carnegie Mellon University, the Chilean Participation Group, the French Participation Group, Harvard-Smithsonian Center for Astrophysics, Instituto de Astrofísica de Canarias, The Johns Hopkins University, Kavli Institute for the Physics and Mathematics of the Universe (IPMU) / University of Tokyo, the Korean Participation Group, Lawrence Berkeley National Laboratory, Leibniz Institut für Astrophysik Potsdam (AIP), Max-Planck-Institut für Astronomie (MPIA Heidelberg), Max-Planck-Institut für Astrophysik (MPA Garching), Max-Planck-Institut für Extraterrestrische Physik (MPE), National Astronomical Observatories of China, New Mexico State University, New York University, University of Notre Dame, Observatário Nacional / MCTI, The Ohio State University, Pennsylvania State University, Shanghai Astronomical Observatory, United Kingdom Participation Group, Universidad Nacional Autónoma de México, University of Arizona, University of Colorado Boulder, University of Oxford, University of Portsmouth, University of Utah, University of Virginia, University of Washington, University of Wisconsin, Vanderbilt University, and Yale University.

## REFERENCES

Abazajian, K. N., Adelman-McCarthy, J., Agueros, M. A., et al. 2009, ApJS, 182, 543

Aguado, D. S., Ahumada, R., Almeida, A., et al. 2019, The Astrophysical Journal Supplement Series, 240, 23, doi: 10.3847/1538-4365/aaf651

- Barrera-Ballesteros, J. K., Heckman, T., Sánchez, S. F., et al. 2018, ApJ, 852, 74, doi: 10.3847/1538-4357/aa9b31
- Behroozi, P., Wechsler, R. H., Hearin, A. P., & Conroy, C. 2019, MNRAS, 1134, doi: 10.1093/mnras/stz1182
- Beygu, B., Kreckel, K., van der Hulst, J. M., et al. 2016, MNRAS, 458, 394, doi: 10.1093/mnras/stw280
- Blanton, M. R., Kazin, E., Muna, D., Weaver, B. A., & Price-Whelan, A. 2011, AJ, 142, 31, doi: 10.1088/0004-6256/142/1/31
- Bond, J. R., Kofman, L., & Pogosyan, D. 1996, Nature, 380, 603, doi: 10.1038/380603a0
- Brown, J. S., Martini, P., & Andrews, B. H. 2016, MNRAS, 458, 1529, doi: 10.1093/mnras/stw392
- Bundy, K., Bershady, M. A., Law, D. R., et al. 2015, ApJ, 798, 7
- Cen, R. 2011, ApJ, 741, 99, doi: 10.1088/0004-637X/741/2/99
- Cooper, M. C., Tremonti, C. A., Newman, J. A., & Zabludoff, A. I. 2008, MNRAS, 390, 245, doi: 10.1111/j.1365-2966.2008.13714.x
- Croton, D. J., Farrar, G. R., Norberg, P., et al. 2005,
  MNRAS, 356, 1155,
  doi: 10.1111/j.1365-2966.2004.08546.x
- da Costa, L. N., Pellegrini, P. S., Sargent, W. L. W., et al. 1988, ApJ, 327, 544, doi: 10.1086/166215
- Di Paolo, C., & Salucci, P. 2018, arXiv e-prints, arXiv:1805.07165. https://arxiv.org/abs/1805.07165
- Douglass, K. A., & Vogeley, M. S. 2017a, ApJ, 834, 186, doi: 10.3847/1538-4357/834/2/186
- —. 2017b, ApJ, 837, 42, doi: 10.3847/1538-4357/aa5e53
- Douglass, K. A., Vogeley, M. S., & Cen, R. 2018, ApJ, 864, 144, doi: 10.3847/1538-4357/aad86e
- Drory, N., MacDonald, N., Bershady, M. A., et al. 2015, AJ, 149, 77, doi: 10.1088/0004-6256/149/2/77
- El-Ad, H., & Piran, T. 1997, ApJ, 491, 421, doi: 10.1086/304973
- Freeman, K. C. 1970, ApJ, 160, 811, doi: 10.1086/150474
- Geller, M. J., & Huchra, J. P. 1989, Science, 246, 897, doi: 10.1126/science.246.4932.897
- Goldberg, D. M., Jones, T. D., Hoyle, F., et al. 2005, ApJ, 621, 643, doi: 10.1086/427679
- Gottlöber, S., Łokas, E. L., Klypin, A., & Hoffman, Y. 2003, MNRAS, 344, 715, doi: 10.1046/j.1365-8711.2003.06850.x
- Grogin, N. A., & Geller, M. J. 2000, AJ, 119, 32, doi: 10.1086/301179
- Hoyle, F., Rojas, R. R., Vogeley, M. S., & Brinkmann, J. 2005, ApJ, 620, 618, doi: 10.1086/427176
- Hoyle, F., & Vogeley, M. S. 2002, ApJ, 566, 641, doi: 10.1086/338340

- Hoyle, F., Vogeley, M. S., & Pan, D. 2012, MNRAS, 426, 3041, doi: 10.1111/j.1365-2966.2012.21943.x
- Kreckel, K., Croxall, K., Groves, B., van de Weygaert, R., & Pogge, R. W. 2015, ApJL, 798, L15, doi: 10.1088/2041-8205/798/1/L15
- Kreckel, K., Platen, E., Aragon-Calvo, M., et al. 2012, AJ, 144, 16, doi: 10.1088/0004-6256/144/1/16
- Martin, G., Kaviraj, S., Laigle, C., et al. 2019, MNRAS, 485, 796, doi: 10.1093/mnras/stz356
- Mateo, M. L. 1998, ARA&A, 36, 435, doi: 10.1146/annurev.astro.36.1.435
- Moorman, C. M., Vogeley, M. S., Hoyle, F., et al. 2015, ApJ, 810, 108, doi: 10.1088/0004-637X/810/2/108
- Moster, B. P., Somerville, R. S., Maulbetsch, C., et al. 2010, ApJ, 710, 903, doi: 10.1088/0004-637X/710/2/903
- Mouhcine, M., Baldry, I. K., & Bamford, S. P. 2007, MNRAS, 382, 801, doi: 10.1111/j.1365-2966.2007.12405.x
- Nakanishi, H., & Sofue, Y. 2006, PASJ, 58, 847, doi: 10.1093/pasj/58.5.847
- Nicholls, D. C., Jerjen, H., Dopita, M. A., & Basurah, H. 2014, ApJ, 780, 88, doi: 10.1088/0004-637X/780/1/88
- Pan, D. C., Vogeley, M. S., Hoyle, F., Choi, Y.-Y., & Park,
  C. 2012, MNRAS, 421, 926,
  doi: 10.1111/j.1365-2966.2011.20197.x
- Park, C., Choi, Y.-Y., Vogeley, M. S., et al. 2007, ApJ, 658, 898, doi: 10.1086/511059
- Patiri, S. G., Prada, F., Holtzman, J., Klypin, A., & Betancort-Rijo, J. 2006, MNRAS, 372, 1710, doi: 10.1111/j.1365-2966.2006.10975.x
- Rojas, R. R., Vogeley, M. S., Hoyle, F., & Brinkmann, J. 2004, ApJ, 617, 50, doi: 10.1086/425225
- —. 2005, ApJ, 624, 571, doi: 10.1086/428476
- Rubin, V. C., & Ford, Jr., W. K. 1970, ApJ, 159, 379, doi: 10.1086/150317
- Sánchez, S. F., Pérez, E., Sánchez-Blázquez, P., et al. 2016, RMxAA, 52, 171
- Sánchez, S. F., Avila-Reese, V., Hernandez-Toledo, H., et al. 2018, RMxAA, 54, 217
- Torres-Flores, S., Epinat, B., Amram, P., Plana, H., & Mendes de Oliveira, C. 2011, MNRAS, 416, 1936, doi: 10.1111/j.1365-2966.2011.19169.x
- Tremonti, C. A., Heckman, T. M., Kauffmann, G., et al. 2004, ApJ, 613, 898, doi: 10.1086/423264
- Tully, R. B., & Fisher, J. R. 1977, A&A, 54, 661
- van de Weygaert, R., & Platen, E. 2011, in International Journal of Modern Physics Conference Series, Vol. 1, International Journal of Modern Physics Conference Series, 41–66
- von Benda-Beckmann, A. M., & Müller, V. 2008, MNRAS, 384, 1189, doi: 10.1111/j.1365-2966.2007.12789.x

Wechsler, R. H., & Tinker, J. L. 2018, ARA&A, 56, 435,

doi: 10.1146/annurev-astro-081817-051756

York, D. G., Adelman, J., Anderson, Jr., J. E., et al. 2000, AJ, 120, 1579, doi: 10.1086/301513